To appear in ApJ
Preprint typeset using LaTeX style emulateapj v. 11/10/09

PROSPECTS FOR MEASURING NEUTRON-STAR MASSES AND RADII WITH X-RAY PULSE PROFILE MODELING

Dimitrios Psaltis[1,2], Feryal Özel[1,2,3], and Deepto Chakrabarty[4]

To appear in ApJ

ABSTRACT

Modeling the amplitudes and shapes of the X-ray pulsations observed from hot, rotating neutron stars provides a direct method for measuring neutron-star properties. This technique constitutes an important part of the science case for the forthcoming *NICER* and proposed *LOFT* X-ray missions. In this paper, we determine the number of distinct observables that can be derived from pulse profile modeling and show that using only bolometric pulse profiles is insufficient for breaking the degeneracy between inferred neutron-star radius and mass. However, we also show that for moderately spinning (300–800 Hz) neutron stars, analysis of pulse profiles in two different energy bands provides additional constraints that allow a unique determination of the neutron-star properties. Using the fractional amplitudes of the fundamental and the second harmonic of the pulse profile in addition to the amplitude and phase difference of the spectral color oscillations, we quantify the signal-to-noise ratio necessary to achieve a specified measurement precision for neutron star radius. We find that accumulating 10^6 counts in a pulse profile is sufficient to achieve a $\lesssim 5\%$ uncertainty in the neutron star radius, which is the level of accuracy required to determine the equation of state of neutron-star matter. Finally, we formally derive the background limits that can be tolerated in the measurements of the various pulsation amplitudes as a function of the system parameters.

Subject headings: stars: neutron — relativity — gravitation

1. INTRODUCTION

When the surface emission from a spinning neutron star is not uniform, a periodic brightness oscillation is produced as the hot and cold spots spin in and out of the line of sight of a distant observer. Such brightness variations may be caused by the magnetic field topology on the stellar surface of a pulsar, by the non-uniform thermonuclear burning on the surface of an X-ray burster, or by the anisotropic accretion of matter from a companion star. The amplitudes and shapes of the resulting pulsations are determined not only by the brightness contours on the stellar surface but also by the degree of strong-field gravitational lensing that photons experience on their paths to the distant observer (Pechenick et al. 1983; Strohmayer et al. 1997). For this reason, pulse profile modeling is a powerful method for measuring neutron-star masses and radii (see Strohmayer 2004). An advantage of this method is that it does not require a measurement of the distance to the neutron star. Two future X-ray missions, NASA's approved *NICER* (Gendreau et al. 2012) and ESA's proposed *LOFT* (Feroci et al. 2012), rely on pulse profile modeling to measure the masses and radii of neutron stars in two classes of sources that show surface brightness oscillations in the X-rays. *NICER* targets the pulsed surface emission that has been detected from rotation-powered millisecond pulsars, while *LOFT* is designed to measure the pulse profiles of accretion-powered millisecond pulsars and of thermonuclear bursters.

Earlier attempts to measure neutron-star properties from rotation-powered (e.g., Pavlov & Zavlin 1997; Bogdanov et al. 2007) and accretion-powered millisecond pulsars (e.g., Poutanen & Gierlinski 2003; Leahy et al. 2008) and bursters (Nath et al. 2002) resulted in large, correlated uncertainties between the inferred masses and radii. *NICER*'s design, which will allow accumulating a large number of counts for each of its targets over very long integration times, and *LOFT*'s large collecting area, which will lead to highly accurate pulse profiles even during the course of a 10 s X-ray burst, will address the issue of reducing the statistical uncertainties of the measurements. However, even when the statistical errors are reduced, significant correlations between the inferred parameters remain. This has been recognized in earlier studies (e.g., Nath et al. 2002; Poutanen & Beloborodov 2006) and has been demonstrated more recently in a detailed study of parameter estimation using mock *LOFT* data (Lo et al. 2013).

In this paper, we use simulated pulse profiles from spinning neutron stars in order to identify the origin of the degeneracies in the measurements of masses and radii that are obtained with this technique. We use a Fourier series decomposition of the pulse profiles at different photon energies to quantify the number of distinct observables that can be measured from each profile. We show that, because gravitational lensing suppresses the amplitudes of the high harmonics, this number is rather small and is practically independent of the number of phase bins used in the measurement. However, the number of independent parameters that are required to uniquely

dpsaltis, fozel@email.arizona.edu, deepto@mit.edu
[1] Astronomy Department, University of Arizona, 933 N. Cherry Ave., Tucson, AZ 85721, USA
[2] Institute for Theory and Computation, Harvard-Smithsonian Center for Astrophysics, 60 Garden St., Cambridge, MA 02138, USA
[3] Radcliffe Institute for Advanced Study, Harvard University, 8 Garden St., Cambridge, MA 02138, USA
[4] Department of Physics and Kavli Institute for Astrophysics and Space Research, Massachusetts Institute of Technology, Cambridge, MA 02139, USA

characterize each system is rather large. Therefore, the effective number of degrees of freedom in comparing theoretical models to data is very small or zero, causing the observed correlations between parameters.

We further demonstrate that obtaining pulse profiles at different photon energies significantly reduces the extent of these correlations. This is because the modulation of the spectrum due to Doppler effects at moderate spin frequencies introduces a photon-energy dependent structure to the pulse profiles. Observing, therefore, pulse profiles in multiple energy bands leads to measuring additional, uncorrelated observables, thereby increasing the effective number of degrees of freedom. The Fourier series decomposition approach that we present here can be used in defining the optimal ranges of photon energies and in formulating analysis strategies that maximize the effective number of degrees of freedom. Moreover, it provides a useful order-of-magnitude estimate for the number of photons that are required to be accumulated and for the level of background that can be accommodated in order for a specified precision to be reached in radius measurements.

2. CALCULATIONS OF PULSE PROFILES

We use the ray tracing algorithm described in Psaltis & Özel (2013) to calculate the brightness oscillations detected by an observer at infinity that arise from a circular, uniform hot spot of angular radius ρ on the surface of a spinning neutron star. The observer and the center of the spot are located at an inclination i and at a colatitude $\theta_{\rm s}$, respectively, with respect to the stellar spin axis. We assume that the emission from the hot spot has a blackbody spectrum and is isotropic in the local Lorentz frame on the stellar surface. Note that, in general, the beaming of the emerging radiation may not be isotropic, but will depend on the particular type of system under consideration (see also end of §3.1).

The targets of interest for missions such as *NICER* and *LOFT* spin at $\sim 200-700$ Hz. The spacetime around such neutron stars can be uniquely described by the Hartle-Thorne metric (Hartle & Thorne 1968). Calculations within this metric allow us to accurately account for the effects of Doppler shifts and aberration, of frame dragging, as well as of the oblateness of the stellar surface and of its quadrupole moment[5]. Morsink et al. (2007) and Psaltis & Özel (2013) showed that all these effects need to be taken into account in order for measurements of neutron-star masses and radii via pulse profile modeling to reach the $\sim 5-10\%$ accuracy required to distinguish between equations of state (e.g., Lattimer & Prakash 2001; Özel & Psaltis 2009).

In this setup, eight distinct parameters are required to fully specify the geometry of the system and the spacetime of a neutron star spinning at a known frequency f:

(i) the mass M of the neutron star;
(ii) the equatorial radius $R_{\rm eq}$ of the neutron star;
(iii) the ellipticity of its surface $\epsilon_{\rm s}$;
(iv) its specific spin angular momentum $a \equiv 2\pi I f c/GM^2$, where I is its moment of inertia;

[5] Simulations of pulse profiles for neutron stars spinning at $\gtrsim$ 700 Hz can only be performed with numerical spacetimes, which depend on the details of the equation of state (see Cadeau et al. 2007 and discussion in Psaltis & Özel 2013).

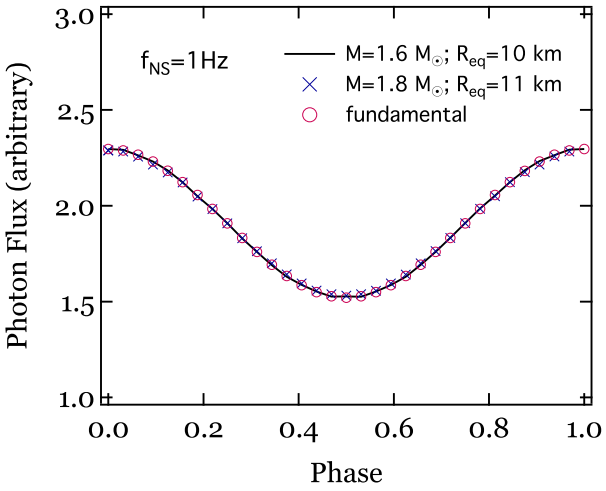

FIG. 1.— Pulse profiles (photon flux as a function of rotational phase) generated by a circular hot spot on the surface of a neutron star spinning at 1 Hz. The solid line corresponds to a neutron star with $M = 1.6M_\odot$ and $R_{\rm eq} = 10$ km and the crosses to a neutron star with $M = 1.8M_\odot$ and $R_{\rm eq} = 11$ km, where we chose the masses and radii so that the two stars have comparable $M/R_{\rm eq}$. The hot spot has a radius of $\rho = 10^\circ$, is located at a colatitude of $\theta_{\rm s} = 40^\circ$, and is observed from an inclination of $i = 30^\circ$ with respect to the stellar spin axis. In order to demonstrate that, at low spin frequencies and for a wide range of geometries, the pulse profile is nearly sinusoidal, we use open circles to show the pulse profile for the 1.6 $M_\odot$ star, when we have suppressed all the harmonics beyond the fundamental. The similarity between all three pulse profiles demonstrates visually that pulse-profile modeling for slowly spinning neutron stars suffers from a large degeneracy between the inferred mass and radius.

(v) the quadrupole moment of its spacetime as measured by the parameter η;
(vi) the observer inclination i;
(vii) the colatitude of the spot $\theta_{\rm s}$; and
(viii) the angular radius of the spot ρ.

If the emission originates from two localized hot spots, as in the case of polar-cap emission from rotation-powered millisecond pulsars (see, e.g., Bogdanov et al. 2007), then up to two additional angles may be needed to specify the relative position of the two spots on the stellar surface.

The observed pulse profiles are affected by each of these eight parameters and could, in principle, contain adequate structure to allow for uncorrelated measurements of all of them. However, as we will show in the following section, gravitational light bending smears the profiles and effectively erases some of the structure that encodes the detailed properties of the neutron star and of the spacetime. As a result, realistic pulse profiles do not contain enough information to measure these eight parameters independently, even at the signal-to-noise ratios expected when a large number of photons is collected.

However, tight relations exist between several of the above macroscopic quantities that depend very weakly on the equation of state (e.g., Morsink et al. 2007; Yagi & Yunes 2013; Bauböck et al. 2013) and can be used to reduce the number of free parameters that are necessary to model pulse profiles. In particular, hereafter, we will use relations that connect the parameters $\epsilon_{\rm s}$, a, and η to M and $R_{\rm eq}$ (Bauböck et al. 2013). Finally, when the angular size of the spot is small ($\rho \lesssim 10^\circ$), the pulse profile does not depend on this parameter (see, e.g., Bog-

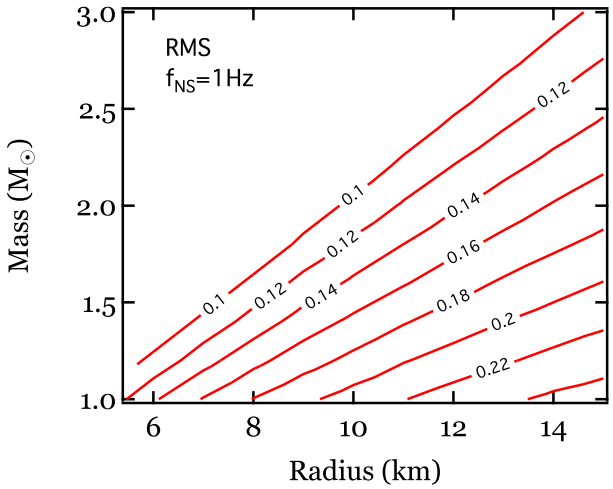

FIG. 2.— Contours of constant fractional rms amplitude of pulsations generated by a hot spot on the surface of a neutron star spinning at 1 Hz, as a function of the assumed stellar mass and radius. The remaining parameters of the calculation are the same as in Figure 1. The contours lie along lines of constant $M/R_{\rm eq}$. This is expected given that the fractional rms amplitude depends on the amount of gravitational lensing experienced by the photons and the latter, for a slowly spinning neutron star, depends only on $M/R_{\rm eq}$.

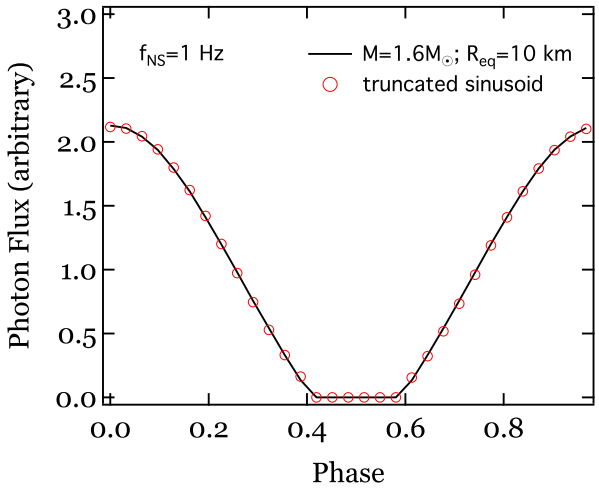

FIG. 3.— Pulse profiles generated by a circular hot spot on the surface of a neutron star spinning at 1 Hz. In this case, the hot spot has a radius $\rho = 10°$, is located at a colatitude $\theta_{\rm s} = 80°$, and is observed from an inclination $i = 90°$ with respect to the spin axis, such that it is occulted by the neutron-star surface for a fraction of the spin period. The solid line shows a truncated sinusoid that best describes the result of the ray-tracing calculation. Even though the occultation generates a large number of measurable harmonics, the pulse profile can be accurately described by only two numbers: its amplitude and the duration of the occultation.

danov et al. 2007). Therefore, for systems in which the surface emission is highly localized, as is expected to be the case during the first fraction of a second of an X-ray burst before the burning front has propagated to a significant distance away from the ignition point (Strohmayer et al. 1997, 1998) and for polar-cap heating in the case of rotation-powered pulsars (e.g., Bogdanov 2013), the spot size can be eliminated as a parameter. As a result, the pulse profile is determined only by four parameters: M, $R_{\rm eq}$, i, and $\theta_{\rm s}$. In the following section, we show that these four parameters can be independently inferred from realistic pulse profiles if we use neutron stars that spin at moderate rates and utilize the photon-energy dependence of the profiles.

3. MEASURING NEUTRON-STAR PARAMETERS FROM PULSE PROFILE MODELING

3.1. *Slowly Spinning Neutron Stars*

The external spacetime of a slowly spinning neutron star depends only on its compactness GM/Rc^2. Therefore, modeling pulse profiles observed from such systems can only lead to a measurement of $M/R_{\rm eq}$ and not of the two parameters independently. We illustrate this degeneracy in Figure 1, where we show the pulse profiles from two slowly spinning (1 Hz) neutron stars, with substantially different masses and radii but with very similar compactness. In Figure 2, we further demonstrate the degenerate dependence of pulse profiles on $M/R_{\rm eq}$. In particular, we plot contours of constant fractional root-mean-squared (rms) amplitude on the mass-radius plane for a neutron star spinning at 1 Hz, while keeping fixed the inclination of the observer to $i = 30°$ and the colatitude of the hot spot to $\theta_{\rm s} = 40°$. As expected, the contours are lines of constant $M/R_{\rm eq}$. In the next section, we will discuss how these contours change as a function of the neutron-star spin frequency.

Figure 1 also demonstrates that the pulse profile is highly sinusoidal by comparing the result of the ray-tracing calculation to a pure sinusoid with the appropriate phase and amplitude. This implies that, even if the signal to noise of an observation allows splitting the observed pulse profile into a large number of phase bins, the complete information content in the profile is captured by a single quantity: the amplitude of the sinusoid. In other words, if we decompose the pulse profile of

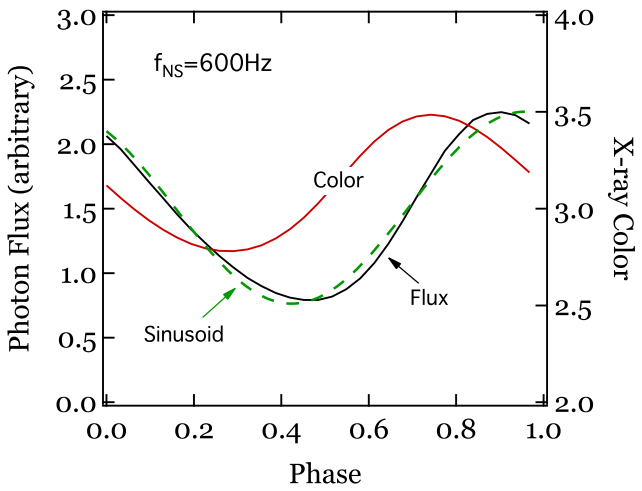

FIG. 4.— The pulse profile and the phase dependence of a spectral color for a neutron star spinning at 600 Hz. In this calculation, the colatitude of the spot is $\theta_{\rm s} = 40°$ and the inclination of the observer is $i = 60°$. The spectral color is defined here as the ratio of the number of photons with energies above the temperature of the blackbody emission to the number of those below. The peak of the spectral color occurs close to the phase at which the tangential velocity of the surface is maximum. On the other hand, the peak of the radiation flux occurs close to the phase at which the projected area of the hot spot is maximum. For this reason, the former precedes the latter. The dashed line shows the sinusoid that has the same amplitude as that of the fundamental harmonic of the oscillations.

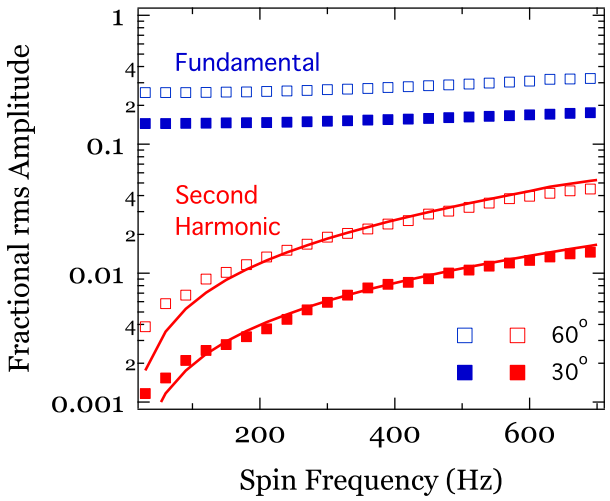

FIG. 5.— Amplitudes of the fundamental and second harmonic for the pulsations originating on the surface of a 1.6 $M_\odot$, 10 km neutron star, as a function of its spin frequency, for two different inclinations of the observer (30° and 60°). The remaining parameters of the calculation are the same as in Figure 1. At slow spins, the pulse profiles are highly sinusoidal whereas, at higher spins, Doppler effects introduce asymmetries to the pulse profiles and increase the amplitudes of the higher harmonics. Even at spin frequencies as high as 600 Hz, the amplitude of the second harmonic is $\simeq 10$ times lower than that of the fundamental for these geometries. The lines show the approximate scaling of equation (1) for the amplitude of the harmonic, given the calculated amplitude of the fundamental. The amplitude of the fundamental increases slightly with spin frequency because of the increase in the peak-to-peak excursion caused by Doppler boosts.

a slowly spinning neutron star into a Fourier series, only the amplitude of the fundamental will be measurable.

When the geometry is such that the hot spot is occulted by the stellar surface for a fraction of the spin phase, a large number of harmonics will be present. However, these additional harmonics acquire large amplitudes only because of the truncation of the otherwise sinusoidal profile due to the occultation (Gibbs phenomenon). In this case, the total information content in the pulse profile is represented by only two quantities, e.g., the fractional rms amplitude of the oscillation and the duration of the occultation (see Fig. 3).

When we compare the number of unique pieces of information encoded in the pulse profile of a slowly spinning neutron star (i.e., two in a geometry with occultation or one without) to the number of parameters required to describe the system (i.e., three: $M/R_{\rm eq}$, i, and $\theta_{\rm s}$), it becomes apparent that pulse profile modeling in such a system can only result in highly correlated measurements of its parameters. Additional structure in the pulse profiles may also be present due to an anisotropic beaming of radiation on the stellar surface (e.g., Poutanen & Beloborodov 2006). However, measuring the amplitudes of the higher harmonics in this case will only provide information about the beaming of radiation and not about the neutron-star properties.

3.2. *Moderately Spinning Neutron Stars*

When a neutron star is spinning at moderate rates ($\sim 300-800$ Hz), the nearly relativistic velocity of its surface causes three phenomena that introduce complexity to the pulse profiles: Doppler shifts of the photon energies, aberration in their angular distribution, and time delays between photons emitted at different spin phases. We show in Figure 4 the deviation of the pulse profile from a pure sinusoid for a spot at 40° colatitude on a neutron star spinning at 600 Hz, and observed from a 30° inclination. As found in earlier studies (e.g., Braje et al. 2000), the pulse profile becomes asymmetric and peaks at an earlier phase compared to the sinusoid.

We quantify the degree of structure in the pulse profiles by comparing the amplitude of the second harmonic to that of the fundamental as a function of the spin frequency in Figure 5. As expected, the amplitude of the second harmonic increases significantly with increasing spin frequency and is more than an order of magnitude larger for a 600 Hz star compared to a slowly spinning one. The harmonic amplitudes also depend strongly on the observer's inclination and are much larger for an observer located closer to the rotational equator. Indeed, the ratio of the harmonic amplitude to that of the fundamental scales approximately as (see Poutanen & Beloborodov 2006)

$$\frac{C_2}{C_1} \simeq 2 \left(\frac{2\pi f R_{\rm eq}}{c} \right) \sin i \sin\theta_{\rm s} = 0.126 \left(\frac{f}{300\ {\rm Hz}} \right) \left(\frac{R_{\rm eq}}{10\ {\rm km}} \right) \sin i \sin\theta_{\rm s} \ . \quad (1)$$

This approximate scaling is shown in Figure 5, for two different observer inclinations, and matches the results of the numerical calculation. Note that the primary scaling is due to the first-order Doppler effect while higher-order corrections (due to the oblateness and the quadrupole moment of the neutron star) affect primarily the numerical factor in this last equation. Using the simpler Schwarzschild+Doppler approximation (e.g., Miller & Lamb 1998; Poutanen & Beloborodov 2006; Lo et al. 2013), as opposed to the Hartle-Thorne metric we use here, therefore, leads only to a systematic bias in the measurement and not to qualitatively different uncertainties.

It is evident from equation (1) that a marked difference between slowly and moderately spinning neutron stars is that in the latter case, the amplitude of the second harmonic shows a strong dependence on the neutron star radius. The amplitudes of higher harmonics can, therefore, be useful for breaking the degeneracy between the stellar mass and radius that we discussed in §3.1. This is shown in Figure 6, in which contours of constant fractional rms amplitude (left panel) and of the ratio of the amplitudes of the second harmonic to the fundamental (right panel) are plotted on the mass-radius parameter space. In this calculation, the neutron star is spinning at 600 Hz, the inclination of the observer is $i = 30°$, and the colatitude of the hot spot is $\theta_{\rm s} = 40°$. (Note that this geometry is far from the one that maximizes the ratio C_2/C_1.) The contours of constant fractional rms amplitude (left panel) are primarily along lines of constant compactness, as in the case of slowly spinning neutron stars. However, they bend upwards at large radii because of the increase in the peak-to-peak flux excursion caused by Doppler boosts. In contrast, the contours of constant amplitude ratios (right panel) are primarily vertical, since the harmonic amplitudes increase with stellar radius, as shown in eq. [1]). The weak mass dependence of these contours

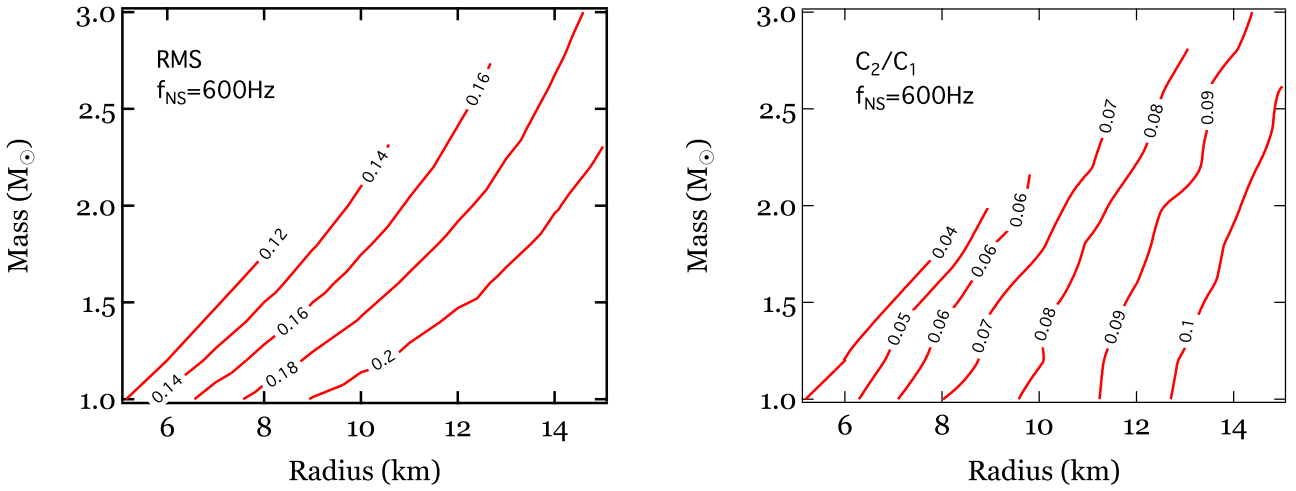

FIG. 6.— Contours of constant *(Left)* fractional rms amplitude and *(Right)* ratio of the amplitude of the harmonic to that of the fundamental for pulsations generated by a hot spot on the surface of a neutron star spinning at 600 Hz, as a function of the stellar mass and radius. The remaining parameters of the calculation are the same as in Figure 1. For a fixed neutron-star spin frequency, the stellar radius determines the magnitude of the Doppler effects, which themselves determine predominantly the harmonic content of the pulse profiles. For this reason, the contours shown in the right panel are nearly vertical and correspond to lines of nearly constant radius.

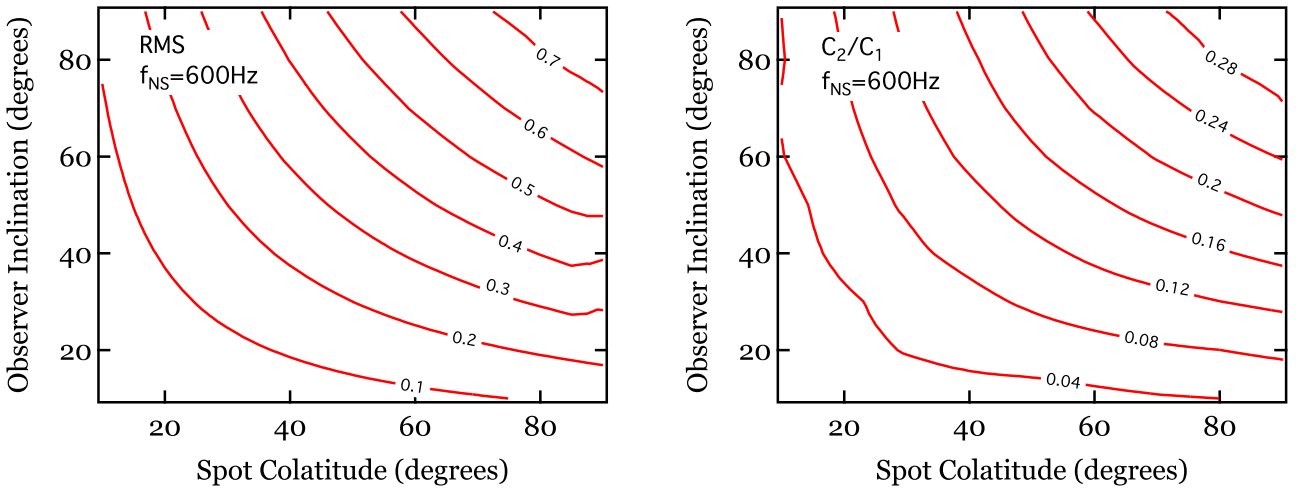

FIG. 7.— Contours of constant *(Left)* fractional rms amplitude and *(Right)* ratio of the amplitude of the harmonic to that of the fundamental for pulsations generated by a hot spot on the surface of a neutron star spinning at 600 Hz, as a function of the colatitude of the spot and the inclination of the observer. The remaining parameters of the calculation are the same as in Figure 1. In both cases, the contours lie primarily along curves on which the product $\sin i \sin\theta_s$ is constant.

arises from the effects of gravitational lensing and from the redshift factors that need to be taken into account when computing the velocity of the stellar surface in the local Lorentz frame.

Figure 5 demonstrates that, even at the high end of the observed spin frequencies, the ratio of the amplitude of the second harmonic to that of the fundamental is quite small; naturally, the amplitudes of the higher harmonics are even smaller (see, e.g., Poutanen & Beloborodov 2006). Moreover, the right panel of Figure 6 shows that the ratio of the amplitude of the harmonic to that of the fundamental needs to be measured to a $\sim 10\%$ fractional accuracy in order for the observations to distinguish between neutron-star radii that differ by ~ 1 km. As we will show in §4, this is quite a severe requirement and makes it unlikely that future observations will be able to extract more than two measurable quantities from bolometric pulse profiles.[6] Therefore, even in this case, the independent pieces of information in realistic measurements still falls short of the number of system parameters (i.e., four) that need to be determined. In principle, the relative phase of the harmonic and the fundamental provides additional information. However, in practice, the phase is too poorly determined due to the weakness of the harmonic.

In Figure 7, we take a different cut through the four-dimensional parameter space and plot the dependence of the fractional rms amplitude (left panel) and the ratio of the amplitude of the harmonic to that of the fundamental (right panel) as a function of the spot colatitude

[6] This number can be increased by one if the geometry of the system is such that the hot spot is occulted for a fraction of the spin phase (see the discussion in §3.1 for the case of slowly spinning neutron stars).

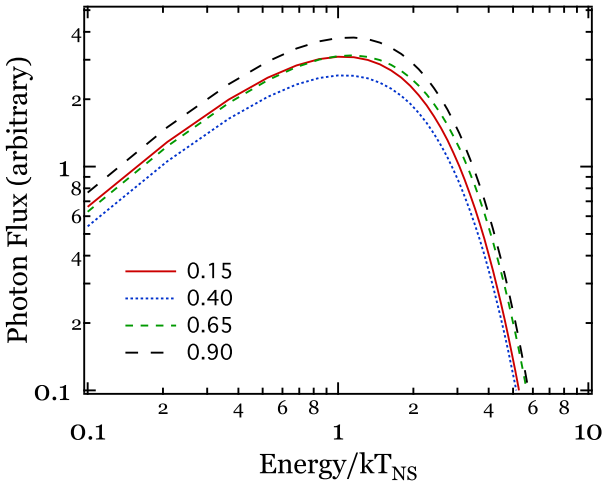

FIG. 8.— The evolution of the radiation spectrum, as observed at infinity at an inclination of 30°, generated by a hot spot on the surface of a neutron star spinning at 600 Hz. The other parameters of the calculation are the same as in Figure 5. The various curves correspond to different spin phases, with zero representing the phase at which the center of the hot spot and the observer are on the same meridian. Comparing the ordering of the curves at very low and very high photon energies reveals a strong color oscillation during a spin cycle.

and the observer's inclination. In both panels, the contours of constant amplitude and the contours of constant harmonic ratio lie along curves on which the product $\sin i \sin\theta_{\rm s}$ is nearly constant. This implies that, if there is no occultation, the two measurable quantities cannot be used to infer the two angles independently. However, given that constraining these two angles independently is often not of interest, the above combination $\sin i \sin\theta_s$ can be treated as a single nuisance parameter, thus reducing the number of system parameters that need to be measured to three. We will now show that the photon energy dependence of the pulse profiles can provide the additional pieces of information and break the remaining degeneracy between parameters.

3.3. *The Photon Energy Dependence of Pulse Profiles*

It is well understood that the Doppler effects that increase the amplitudes of the higher harmonics in the pulse profile also introduce a modulation to the radiation spectrum observed at infinity. This is shown for a typical set of parameters in Figure 8 at four different spin phases. As expected, the radiation spectrum is softer in the range of spin phases for which the hot spot is receding from the observer and harder when the hot spot is approaching.

We can quantify the degree of spectral modulation during a pulse phase by defining a color as the ratio between the number of photons observed in two energy bands separated at an energy equal to the hot-spot temperature. In Figure 4, we plot the evolution of such a color with pulse phase for a typical configuration, where we use a photon energy equal to the hot-spot temperature (as measured at the neutron-star surface) to separate the two energy bands. The evolution of the color with pulse phase shows a nearly sinusoidal modulation with a significant fractional rms amplitude and a peak phase that is offset from that of the flux oscillation. As we will show below, the amplitudes and the peak phases of the color oscillations do not have the same dependence on the system parameters as the amplitudes of the harmonics of the bolometric flux. For this reason, they provide the two additional observables needed to break the degeneracies discussed in §3.2 and allow a measurement of all the system parameters. This is true even when using the minimal spectral information encoded in one spectral color. If the number of photons accumulated during an observation allow separating the pulse profiles into several energy bands, additional consistency relations between model parameters can be obtained.

Figure 9 shows contours of constant fractional rms amplitude of the color oscillations (left panel) and of the phase difference between the phase of peak color minus the phase of peak flux (right panel) on the mass-radius parameter space. If there were no gravitational lensing and redshift effects, the amplitude of the color oscillations would be strictly proportional to the radius of the neutron star and would have a scaling similar to the one given in equation (1). However, gravitational effects introduce a weak dependence on the neutron-star compactness such that the contours of constant color amplitude shown in Figure 9 are not parallel to the contours of constant harmonic ratios shown in the right panel of Figure 6.

The dependence of the contours of constant phase difference between the color and flux oscillations on mass and radius shown in the right panel of Figure 9 is more subtle. The peak phases of the two oscillations are determined by the combination of the evolution of the projected surface area of the hot spot on pulse phase (which peaks at phase zero) and of the Doppler effects (which peak at phase 0.75). The flux oscillation is determined predominantly by the former effect, peaks close to zero phase, and the Doppler boosts introduce small corrections, moving the peak toward earlier phases. On the other hand, the color oscillation is determined predominantly by the Doppler effects, peaks close to phase 0.75, and the surface area projection introduces a small correction, moving the peak toward later phases. For small values of the neutron-star compactness, for which the gravitational lensing effects are weak, the relative shift between the two peak phases is dominated by Doppler effects and, therefore, the contours shown in Figure 9 become more vertical. At high values of the neutron-star compactness, for which the relative shift between the two peak phases is dominated by gravitational lensing effects, the contours become nearly horizontal.

The contours of the four observables shown in Figures 6 and 9 on the mass-radius parameter space do not have the same dependence on the system properties. This leads to the conclusion that measuring with sufficient accuracy the amplitudes of the lowest two harmonics of the bolometric flux oscillation, as well as the amplitude and relative phase of the spectral color oscillation is adequate to uniquely determine all four parameters of each observed system, as we will discuss in the next section.

We explore in Figure 10 the dependence of the fractional rms amplitude of the color oscillations (left panel) and the phase difference between the flux and the color oscillations (right panel) on the spot colatitude and the inclination of the observer. The contours of constant fractional rms color amplitude lie along curves on which the product $\sin i \sin\theta_{\rm s}$ is nearly constant, as was the case

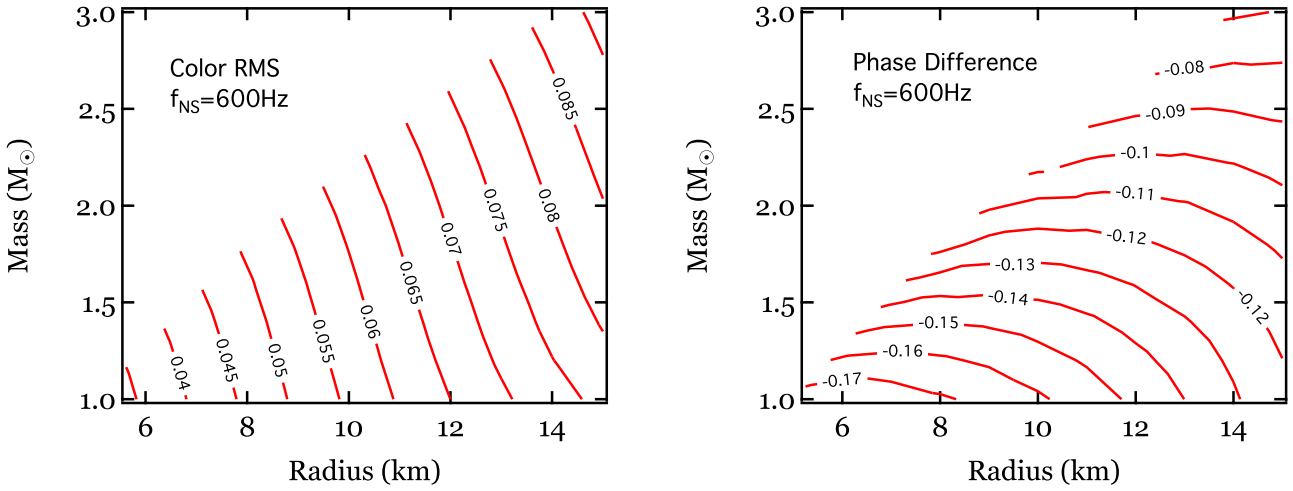

FIG. 9.— Contours of constant *(Left)* fractional rms amplitude of a spectral color oscillation and *(Right)* difference between the phase of peak spectral color and of peak radiation flux, for pulsations generated by a hot spot on the surface of a neutron star spinning at 600 Hz, as a function of the stellar mass and radius. The remaining parameters of the calculation are the same as in Figure 8. The color oscillations are introduced primarily by Doppler effects and, therefore, the contours on the left panel are nearly vertical, as in the right panel of Figure 6. Understanding the shape of the contours in the right panel of this figure is more subtle and is described in detail in the text.

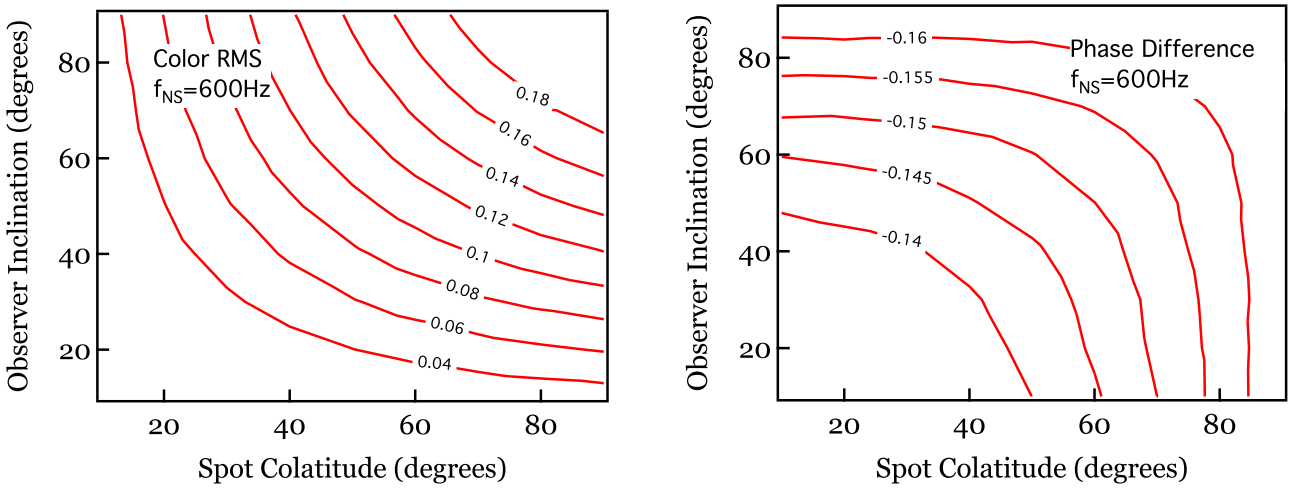

FIG. 10.— Contours of constant *(Left)* fractional rms amplitude of a spectral color oscillation and *(Right)* difference between the phase of peak spectral color minus that of peak radiation flux, for pulsations generated by a hot spot on the surface of a neutron star spinning at 600 Hz, as a function of the colatitude of the spot and the inclination of the observer. The remaining parameters of the calculation are the same as in Figure 8. The contours of the fractional rms amplitude of the spectral oscillation approximately follow curves on which the product $\sin i \sin\theta_s$ is constant, as in the case of the first two observables shown in Figure 7. In contrast, the phase difference results in a nearly orthogonal constraint and provides the information needed to measure the two angles independently.

with the two observables obtained from the bolometric flux oscillations (see Fig. 7). This is expected given that the color oscillations are also generated by Doppler effects and are determined by the projection of the vector of the surface velocity along the instantaneous line-of-sight between the observer and the hot spot. In contrast, the phase difference between the flux and the color oscillations shows a significantly different dependence on the two angles. Therefore, if measuring the two angles independently is a goal in and of itself, this last observable provides the additional piece of information necessary to achieve it.

4. PROSPECTS FOR MEASURING NEUTRON-STAR PROPERTIES FROM PULSE PROFILE MODELING

In §2, we showed that the pulse profile observed from a neutron star spinning at a moderate rate can be accurately described by four parameters: the mass of the neutron star, its equatorial radius, the inclination of the observer, and the colatitude of the hot spot on the stellar surface. In §3, we demonstrated that observations of the photon energy dependent pulse profiles result in at least four measurable quantities that have a distinct dependence on the model parameters: the amplitude of the bolometric flux oscillation, the amplitude of its second harmonic, the amplitude of the spectral color oscillation, and the phase difference between the bolometric flux and the color oscillations.

The first three of these four observables depend on the same combination $\sin i \sin\theta_s$ of the two geometric parameters. Therefore, if the main goal of the pulse profile modeling is to measure the masses and radii of neutron stars, this combination can be treated as a sin-

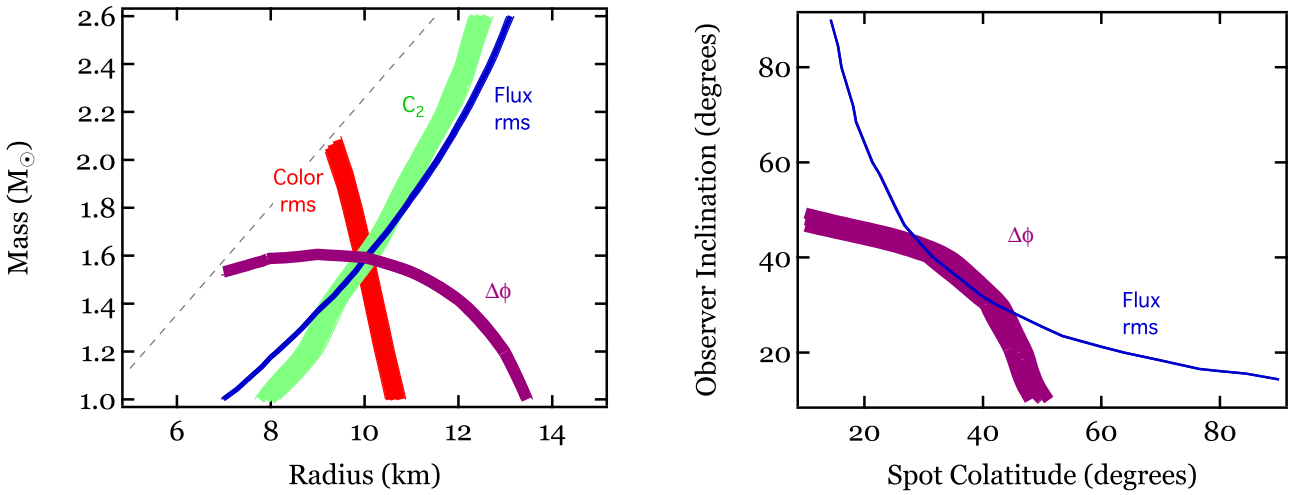

FIG. 11.— Constraints on *(Left)* the neutron-star mass and equatorial radius and *(Right)* the inclination of the observer and colatitude of the hot spot, obtained from measuring four properties of a pulse profile. The measured values of the fractional rms amplitude of the pulse profile, the fractional rms amplitude C_2 of the harmonic, the fractional rms amplitude of the color oscillation, and the phase difference $\Delta\phi$ between the flux and color oscillations were assumed to be equal to 0.17 ± 0.005, 0.018 ± 0.001, 0.058 ± 0.001, and -0.136 ± 0.002, respectively. The central values for each parameter correspond to the results of the calculation for a 1.6 $M_\odot$, 10 km neutron star, observed from an inclination of 30°, with a hot spot on its surface at a colatitude of 40°. Each panel represents a cut through the four-dimensional parameter space on which the parameters not shown remain constant. The distinct dependence of the four observables on the system parameters allows a unique recovery of the assumed neutron-star mass and radius.

gle parameter. In this case, the first three observables lead to a unique determination of the system parameters. Nonetheless, if all four observables can be measured with sufficient accuracy, then the geometry of the system can also be uniquely determined.

In §3, we also quantitatively explored the dependence of the four observables on the neutron star mass and radius. Three of the four observables acquire detectable amplitudes because of the relativistic Doppler shifts on the rapidly spinning neutron-star surface. As a result, the accuracy of the measurements will depend on the accuracy at which the amplitudes of the harmonics and color oscillations can be measured. Using, for example, equation (1), we can relate an uncertainty ΔC_2 for the measurement of the amplitude of the harmonic to an uncertainty for the inferred radius $\Delta R_{\rm eq}$ as

$$\frac{\Delta R_{\rm eq}}{R_{\rm eq}} = \left[2 C_1 \left(\frac{2\pi f R_{\rm eq}}{c} \right) \sin i \sin \theta_{\rm s} \right]^{-1} \Delta C_2 \ . \qquad (2)$$

As we show in the appendix, the uncertainty with which the amplitude of a given harmonic can be measured depends on the total number of source counts S accumulated during the observations and on the total number of background counts B accumulated at the same time as

$$\Delta C_n = \frac{\sqrt{S+B}}{S} \ . \qquad (3)$$

Combining the last two equations, we obtain

$$\frac{\Delta R_{\rm eq}}{R_{\rm eq}} = \left[\left(\frac{4\pi f R_{\rm eq}}{c} \right) \sin i \sin \theta_{\rm s} \right]^{-1} \left(\frac{\sqrt{S+B}}{C_1 S} \right) \ . \qquad (4)$$

This equation provides the analytic understanding for the figure of merit $\mathcal{R}$ introduced by Lo et al. (2013), which is closely related to the quantity in the rightmost parentheses shown above.

When the number of source photons dominates that of the background, i.e., when $S \gg B$, then the uncertainty in the measurement of the neutron-star radius scales as

$$\frac{\Delta R_{\rm eq}}{R_{\rm eq}} \simeq 0.055 \left(\frac{C_1}{0.3} \right)^{-1} \left(\frac{f}{600\ {\rm Hz}} \right)^{-1} \left(\frac{R_{\rm eq}}{10\ {\rm km}} \right)^{-1} \left(\frac{\sin i}{0.5} \right)^{-1} \left(\frac{\sin \theta_{\rm s}}{0.5} \right)^{-1} \left(\frac{S}{10^6\ {\rm cts}} \right)^{-1/2} \qquad (5)$$

This relation suggests that achieving a 5% accuracy in the measurement of a neutron star radius from pulse profile modeling requires accumulating of the order 10^6 source counts.

Figure 11 shows the constraints on the model parameters that can be obtained from measuring the four observable quantities discussed above with a precision that is characteristic of an observation with one million source counts. In particular, we assumed that all fractional amplitudes were measured with an accuracy of 10^{-3} and the phase difference between flux and color oscillations was measured with an accuracy of 5×10^{-4} (see the Appendix). For this example, the simulated lightcurve was generated for a $1.6 M_\odot$, 10 km neutron star spinning at 600 Hz, observed at an inclination of 30°, with a small uniform hot spot on its surface at a colatitude of 40°. The figure demonstrates that the distinct dependence of the four observables on the system parameters allows a unique recovery of the assumed neutron-star mass and radius. Moreover, it also shows that the assumed uncertainties lead to a measurement of the neutron star mass and radius that is sufficient to distinguish between different equations of state.

4.1. *Importance of the Background Model*

We emphasize that three of the four observables discussed above are fractional rms amplitudes of Fourier harmonics. Measuring these fractional amplitudes requires obtaining both the pulsed and unpulsed ("DC") components of the pulse profiles. If an additional background that does not originate on the neutron-star sur-

face is present in the observed energy band, this component needs to be separately measured and subtracted. The alternative, i.e., measuring the properties of the additional background from the pulse profiles themselves, introduces severe degeneracies between the inferred model parameters, as shown in Lo et al. (2013). This is easy to understand within the framework of counting system parameters and observables that we followed here. Indeed, if we choose to perform pulse profile analysis in two energy bands with unknown backgrounds, then we introduce two additional parameters to our model, increasing the total number to six. However, the number of observables that can be inferred accurately from the pulse profiles remains equal to four. This difference between the number of model parameters and observables results in substantial degeneracies between the model parameters of interest.

The approach we developed in this paper allows us to also investigate the accuracy at which the number of background counts needs to be known *a priori* in order for a desired accuracy in the mass and radius measurement to be achieved. If we denote by a_n the absolute amplitude of the $n-$th Fourier component in a profile and by $N \equiv S + B$ the total number of counts accumulated, then the fractional source amplitude of the same Fourier component is simply

$$C_n = \frac{a_n}{S} = \frac{a_n}{N-B} \ . \tag{6}$$

At least two effects, in principle, contribute to the uncertainty in the measurement of the fractional source amplitude: the uncertainty in the measurement of the absolute amplitude Δa and the uncertainty in the *a priori* knowledge of the background ΔB. Incorporating both sources of error, we obtain

$$\begin{aligned} \Delta C_n^2 &= \frac{\Delta a_n^2}{(N-B)^2} + \left[\frac{a_n}{(N-B)^2}\right]^2 \Delta B^2 \\ &= \left(\frac{\Delta a_n}{S}\right)^2 + \left(\frac{a_n}{S^2}\right)^2 \Delta B^2 \ . \end{aligned} \tag{7}$$

The first term in the right-hand side of this equation is the Poisson error in the measurement of the fractional amplitude and is given by equation (3). Assuming that the uncertainty in the measurement of the background is Poisson dominated, $\Delta B = \sqrt{B}$. Inserting these two expressions in the last equation, we obtain

$$\Delta C_n^2 = \left(\frac{\sqrt{S+B}}{S}\right)^2 + C_n^2 \frac{B}{S^2} \tag{8}$$

or simply

$$\Delta C_n = \frac{\sqrt{S + B(1+C_n^2)}}{S} \ . \tag{9}$$

Equation (9) shows that the background contributes in two ways in the uncertainty of the measured fractional amplitude of the source: the overall counts in the background increase the level of the Poisson noise in the power spectrum and hence degrade the measurement of the absolute amplitude of the pulsations. At the same time, the uncertainty in the subtraction of the background counts affects the inference of the fractional amplitude of the pulsations. Because $C_n^2 \ll 1$, the latter effect is always subdominant compared to the former. We can, therefore, neglect it and simply use equation (4) to infer the expected uncertainty in the measurement of neutron-star radii when the observations have a significant background.

5. CONCLUSIONS

In this paper, we investigated how pulse profiles generated by hot spots on moderately spinning neutron stars can be used to infer the stellar mass and radius. We showed that bolometric pulse profiles do not contain sufficient information to break parameter degeneracies to uniquely measure these quantities. However, a measurement of the spectral color oscillations provides additional constraints that allow a separate determination of M and $R_{\rm eq}$. Extracting pulse profiles even in just two different energy bands is sufficient to derive this information. However, achieving 5% precision in neutron-star radius requires accumulating $\gtrsim 10^6$ counts in the pulse profile measurements. This can be accomplished by long exposure times (as in the case of *NICER*) or by a large collecting area (as in the case of *LOFT*).

The requirements we presented here for making measurements of the neutron star radius with a given precision are robust to the detailed energy coverage and response of a particular instrument. Given that our study has utilized idealized light curves, the details of, e.g., required number of counts, can be refined for a particular detector or choice of energy bandpass. However, we note that because only two energy channels are required to make the spectral color oscillation measurement, even a modest energy resolution is sufficient. On the other hand, a broad energy coverage is advantageous because the color oscillations are more pronounced when measured over a wider energy range. Ideally, the energy bandpass should include at least the blackbody peak or the exponential tail above the peak.

X-ray spectral color oscillations have been previously reported in several thermonuclear burst oscillations from two neutron stars (Strohmayer et al. 1999; Strohmayer 2000). These color oscillations were all measured during the burst decay phase and were found to be in phase with the flux oscillations, contrary to the expectations discussed above. This suggests that the color oscillations in the burst tails are not generated by Doppler effects and are not appropriately modeled by the hot spot model described above. This also corroborates other lines of arguments that the oscillations in the burst tail are generated by a different mechanism (e.g., surface modes) than those in the burst rise (see also Watts 2012 and references therein).

In the case of oscillations observed during the rise phases of X-ray bursts, which are the prime targets for *LOFT*, the predominant background arises from the X-ray emission from the accretion flow. In the case of surface emission from rotation powered pulsars, which are the main targets for *NICER*, the non-thermal emission from the neutron-star magnetosphere is the main source of the background. In both cases, the energy spectrum of the pulsations is very different from the energy spectrum of the background. If the shape of the energy spectrum of the background is known, e.g., from theoretical models and prior observations, then its overall normalization

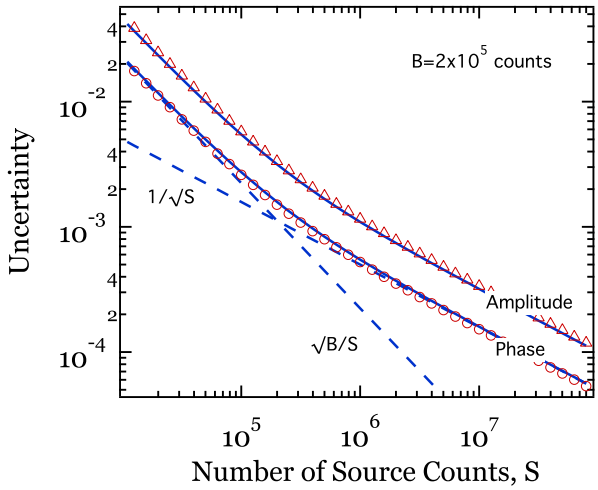

FIG. 12.— The dependence of the uncertainty in the measured amplitude *(triangles)* and phase *(circles)* of a periodic signal on the number of photons, S, detected from a source. For the simulations shown in this Figure, the number of background photons was set to $B = 2 \times 10^5$. The solid lines show the two analytic expression for the uncertainties, as given in the text. When the observation is background-dominated, the uncertainty scales as $\sqrt{B}/S$ whereas, when it is source-dominated, it scales as $1/\sqrt{S}$.

can be measured at an energy band where the pulsed surface emission is negligible, i.e., at hard X-rays. Such an approach will lead to an independent measurement of the background in the energy bands of interest and will not adversely affect measuring neutron-star masses and radii from pulse profile modeling.

We thank the *NICER* and *LOFT* science teams for many discussions on ray tracing in neutron-star spacetimes. This work was supported in part by NSF grant AST-1108753, NSF CAREER award AST-0746549, and *Chandra* Theory grant TM2-13002X. F.Ö. gratefully acknowledges support from the Radcliffe Institute for Advanced Study at Harvard University. D.P. and F.Ö. thank the Institute for Theory and Computation at Harvard University for their hospitality during the time that this work was completed.

APPENDIX

UNCERTAINTIES IN THE MEASUREMENT OF PULSATION AMPLITUDES AND PHASES

In this appendix we show, for completeness, that the accuracy with which the fractional amplitude and phase of a periodic signal can be measured from a noisy time series that is folded at the known period of the signal depends on the total number of counts due to the source and due to the known background (see also discussion in van der Klis 1989).

Because of Poisson noise in the measurement, the amplitudes of the Fourier components of a signal that is assumed to be constant in time are not zero. If we denote by x_k the number of photons measured in the k-th bin of such a time series and by a_j the Fourier component at frequency bin j, where $n_{\rm b}$ is the number of bins, we can write

$$x_k = \frac{1}{n_{\rm b}} \sum_{j=-n_{\rm b}/2}^{n_{\rm b}/2} a_j \exp\left(-2\pi i j k/n_{\rm b}\right) \ . \tag{A1}$$

The mean number of photons in each bin is

$$\bar{x}_k = \frac{a_0}{n_{\rm b}} = \frac{S+B}{n_{\rm b}} \ , \tag{A2}$$

where we have denoted by S and B the total number of photons collected due to the source and due to the background, respectively.

Poisson noise leads to a flat Fourier spectrum with a mean amplitude that we denote here by $a_{\rm P}$. We can calculate this mean amplitude using Parseval's theorem. The variance in the number of counts collected in each time bin is related to the Fourier amplitudes by

$$\mathrm{Var}(x_k) = \frac{1}{n_{\rm b}} \sum_{j=-n_{\rm b}/2; j\neq 0}^{n_{\rm b}-1} |a_j|^2 \simeq |a_{\rm P}|^2; . \tag{A3}$$

Moreover, the standard deviation σ of the number counts in each bin is related to the mean number of photons by $\sigma^2 = \bar{x}_k$ and to the variance by

$$\sigma^2 = \frac{\mathrm{Var}(x_k)}{n_{\rm b}} \ . \tag{A4}$$

Combining the last two equations together, we find that the mean amplitude of the Fourier components of the Poisson noise is

$$|a_{\rm P}| = \frac{\sqrt{S+B}}{n_{\rm b}} \ . \tag{A5}$$

If the time series contains in addition to the Poisson noise a periodic signal that is uncorrelated with the noise, the quantity $|a_{\rm P}|$ will represent the uncertainty within which the amplitude of the signal can be measured.

In this paper, we have been using fractional amplitudes of the periodic signals, which we can obtain by dividing the absolute amplitude of a signal by the average number of counts in each bin due to the source alone. In this case, the noise level $C_{\rm P}$ of the fractional amplitudes becomes

$$C_{\rm P} = \left(\frac{|a_{\rm P}|}{n_{\rm b}}\right)\left(\frac{S}{n_{\rm b}}\right)^{-1} = \frac{\sqrt{S+B}}{S} \ . \tag{A6}$$

In order to verify the validity of equation (A6), we generated a large number of simulated observations using the lightcurve shown in Figure 4 for a different number of source photons S and a constant background of $B = 2{\times}10^5$ counts, adding the appropriate level of Poisson noise. For each simulated observation, we measured the amplitude of the fundamental and of the second harmonic and used the distribution of amplitudes over the various realizations to infer the uncertainty in each measurement. The open triangles in Figure 12 show the measured uncertainty of the amplitudes as a function of the number of source counts. The solid line that follows the open triangles is the analytic result of equation (A6) and agrees well with the results of the simulations.

We used the same simulations to also measure the phase of the fundamental Fourier component with respect to a fiducial phase in all realizations of the data. The open circles in Figure 12 show the dependence of the uncertainty in the measured phase on the number of source counts. The solid line that follows the open circles is given by the simple relation

$$\sigma_\phi = \frac{\sqrt{S+B}}{2S} \tag{A7}$$

and also agrees well with the results of the simulations.

REFERENCES

Bauböck, M., Berti, E., Psaltis, D., Özel, F. 2013, ApJ, 777, 68
Bogdanov, S., Rybicki, G. B., & Grindlay, J. E. 2007, ApJ, 670, 668
Bogdanov, S., ApJ, 762, 96
Braje, T. M., Romani, R. W., & Rauch, K. P. 2000, ApJ, 531, 447
Cadeau, C., Morsink, S. M., Leahy, D., & Campbell, S. S. 2007, ApJ, 654, 458
Feroci, M., Stella, L., van der Klis, M., et al. 2012, Experimental Astronomy, 34, 415
Gendreau, K. C., Arzoumanian, Z., & Okajima, T. 2012, Proc. SPIE, 8443, 844313
Hartle, J. B., & Thorne, K. S. 1968, ApJ, 153, 807
Lattimer, J. M., & Prakash, M. 2001, ApJ, 550, 426
Leahy, D. A., Morsink, S. M., & Cadeau, C. 2008, ApJ, 672, 1119
Lo, K. H., Miller, M. C., Bhattacharyya, S., & Lamb, F. K. 2013, ApJ, 776, 19
Miller, M. C., & Lamb, F. K. 1998, ApJ, 499, L37
Morsink, S. M., Leahy, D. A., Cadeau, C., & Braga, J. 2007, ApJ, 663, 1244
Nath, N. R., Strohmayer, T. E., & Swank, J. H. 2002, ApJ, 564, 353
Özel, F., & Psaltis, D. 2009, Phys. Rev. D, 80, 103003
Pavlov, G. G., & Zavlin, V. E. 1997, ApJ, 490, L91
Pechenick, K. R., Ftaclas, C., & Cohen, J. M. 1983, ApJ, 274, 846
Poutanen, J., & Beloborodov, A. M. 2006, MNRAS, 373, 836
Poutanen, J., & Gierliński, M. 2003, MNRAS, 343, 1301
Psaltis, D., & Özel, F. 2013, ApJ, submitted, arXiv:1305.6615
Strohmayer, T. E. 2000, AIP Conf. Proc. 522, Cosmic Explosions, ed. Zhang, W. W. & Holt, S. S. (Melville, NY: AIP), 375
Strohmayer, T. E. 2004, AIP Conf. Proc. 714, X-ray Timing 2003: Rossi and Beyond, ed. Kaaret, P., Lamb, F. K., & Swank, J. H. (Melville, NY: AIP), 245
Strohmayer, T. E., Swank, W., & Zhang, W. 1999, Nucl.Phys.B Proc.Suppl, 69, 129
Strohmayer, T. E., Zhang, W, & Swank, J. H. 1997, ApJ, 487, L77
Strohmayer, T. E., Zhang, W, Swank, J. H., White, N. E., & Lapidus, I. 1998, ApJ, 498, L135
van der Klis, M. 1989, Timing Neutron Stars, eds. H. Ogelman and E.P.J. van den Heuvel. NATO ASI Series C, Vol. 262, p. 27-70. Dordrecht: Kluwer, 1989., 27
Watts, A. L. 2012, ARA&A, 50, 609
Yagi, K., & Yunes, N. 2013, Phys. Rev. D, 88, 023009